Jurnal Teknologi

Full Paper

SUPERIOR ANTIBACTERIAL PROPERTIES OF COPPER-BEARING HIGH ENTROPY ALLOY COATED STAINLESS STEEL SURFACE FABRICATED USING LASER CLADDING

Nazar Khalaf Mahan[a,c], Mohammed Faraj Al Marjani[c], Muhammad Safwan Abd Aziz[a,b], Abdul Rahman Johari[a,b], Siti Qistina Arora Talib[a,b], Ganesan Krishnan[a,b*]

[a]Department of Physics, Faculty of Science, Universiti Teknologi Malaysia, 81310 UTM Johor Bahru, Johor, Malaysia
[b]Laser Center, Ibnu Sina Institute for Scientific & Industrial Research (ISI-SIR), Universiti Teknologi Malaysia, 81310 UTM Johor Bahru, Johor, Malaysia
[c]Department of Physics, College of Science, Mustansiriyah University, Baghdad, Iraq

Article history
Received
24 January 2024
Received in revised form
3 June 2024
Accepted
23 July 2024
Published Online
17 October 2024

*Corresponding author
k.ganesan@utm.my

Graphical abstract

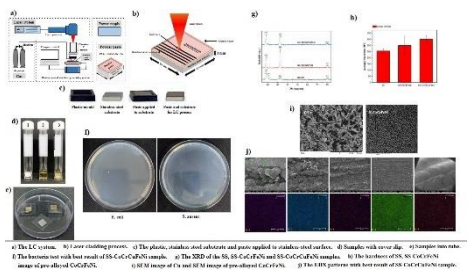

Abstract

A high-entropy alloy (HEA) coating is applied to a stainless-steel surface using the laser cladding (LC) process. This coating offers a broad-spectrum antibacterial ability and favorable mechanical properties. The release of copper ions from the HEA effectively inhibits the growth of Gram-negative *Escherichia coli* (*E. coli*) and Gram-positive *Staphylococcus aureus (S. aureus),* enhancing the alloy's suitability for various applications requiring antibacterial properties. The elemental compositions, sizes, and morphologies of the constructed HEAs are revealed through X-ray diffraction (XRD), scanning electron microscopy (SEM), and energy dispersive X-ray analysis (EDX). This study validates the feasibility of applying the antibacterial CoCrFeCuNi HEA alloy coating to stainless steel via LC. The antibacterial evaluation showcases the enhanced efficacy of the CoCrCuFeNi HEA coating, demonstrating an antibacterial effectiveness of approximately 89% against *E. coli* and 98% against *S. aureus*. In contrast, the CoCrFeNi HEA coating exhibits an antibacterial effectiveness of about 40% against *E. coli* and 93% against *S. aureus*. The Vickers hardness of the stainless steel coated with CoCrCuFeNi HEA has significantly increased to 352 HV, compared to the CoCrFeNi coating with a hardness of 300.6 HV and the uncoated stainless steel with a hardness of 256.6 HV. This HEA alloy demonstrates considerable potential for use in medical applications or other settings that require antibacterial features.

Keywords: Stainless steel, Antibacterial activity, High entropy alloy, In-situ alloying, Laser cladding

Abstrak

Salutan aloi entropi tinggi (HEA) CoCrFeCuNi disalutkan pada permukaan keluli tahan karat melalui proses penyalutan laser (LC). Penyalutan ini menyumbang kepada kebolehan antibakteria berspektrum luas dan faedah sifat mekanikal. Pengeluaran ion kuprum dari HEA berkesan menghalang pertumbuhan *Escherichia coli* (*E. coli*) gram-negatif dan *Staphylococcus*

aureus (*S. aureus*) gram-positif, mempertingkat kesesuaian aloi dalam pelbagai aplikasi yang memerlukan sifat antibakteria. Komposisi unsur, saiz, dan morfologi HEA yang dibina ditampilkan dengan menggunakan belauan sinar-X (XRD), mikroskop elektron pengimbasan pancaran (SEM), dan analisa spektroskopi sinar-X sebaran tenaga (EDX). Kajian ini mengesahkan kebolehlaksanaan penggunaan HEA CoCrFeCuNi antibakteria pada keluli tahan karat melalui LC. Penilaian antibakteria mendemonstrasikan keberkesanan tertingkat bagi salutan HEA CoCrCuFeNi, mempamerkan keberkesanan antibakteria kira-kira 89% terhadap E. coli dan 98% terhadap S. aureus. Sebaliknya, salutan HEA CoCrFeNi menunjukkan keberkesanan antibakteria sebanyak 40% terhadap E. coli dan 93% terhadap S. aureus. Ujian kekerasan Vickers terhadap keluli tahan karat yang disalutkan HEA CoCrCuFeNi menaik dengan ketara sehingga 352 HV berbanding dengan salutan CoCrFeNi dengan kekerasan 300.6 HV dan keluli tahan karat tidak bersalut dengan kekerasan 256.6 HV. Aloi HEA mempamerkan potensi yang tinggi untuk kegunaan dalam aplikasi perubatan atau persekitaran lain yang memerlukan sifat antibakteria.

Kata kunci: Keluli tahan karat, Aktiviti antibakteria, Aloi entropi tinggi, Pengaloian in-situ, Pelapisan laser

1.0 INTRODUCTION

Stainless steel is commonly used in hospitals as a metallic biomaterial due to its easy maintenance, durability, and aesthetic appeal. However, for more challenging applications, the material requires surface cleaning because it lacks adequate antibacterial properties [1]. While surface disinfectants can be used to clean contaminated surfaces, this solution is temporary, necessitating frequent reapplication to maintain a bacteria-free environment. In 2020, the global sales of surface disinfectants reached USD 4.5 billion, indicating a 30% increase from the previous year [2]. Typically, a surgical site may show signs of superficial infections that affect the skin and subcutaneous tissues within a month after surgery. To ensure patient safety, surgical instruments such as knives and needles, are subjected to several mandatory processes before use. These processes include cleaning, disinfection, and sterilization, which are crucial steps taken to uphold the highest level of hygiene and minimize the risk of infection [3–5]. Medical devices can be broadly categorized into three groups based on their application and purpose: surgical tools, implanted medical devices, and interventional medical devices [6]. In recent years, there has been a growing interest in applying material coatings to medical equipment, primarily stainless steel instruments such as knives, scissors and needles. This strategy enables the modification of surface properties without affecting the underlying biomechanical characteristics of the equipment [7–9]. The coatings must fulfill several criteria, including resistance to wear and cleaning, antibacterial properties, low light reflection, and biocompatibility.

In 2004, Yeh *et al*. introduced High Entropy Alloys (HEAs), a novel material that composed of five to thirteen principal elements [10–12]. These elements exist in nearly equimolar proportions, with concentrations ranging from five to thirty-five percent (at%). Due to their unique properties, such as the high entropy effect, lattice distortion effect, delayed diffusion effect, and cocktail effect [13], HEAs have attracted significant attention from researchers. These properties contribute to the material's favorable attributes, such as high strength, high hardness, good wear resistance, corrosion resistance, and other benefits [14–16]. By utilizing the concept of HEAs, a novel antibacterial HEA has been developed through the incorporation of various elements. Copper (Cu) imparts antibacterial properties, Iron is added to enhance formability, chromium enhances corrosion resistance, and nickel helps prevent brittleness. This antibacterial alloy is designed to maintain exceptional mechanical properties, including high strength, superior hardness, excellent wear resistance, and corrosion resistance [17]. Zhou *et al*. designed a unique alloy, denoted as $Al_{0.4}$CoCrCuFeNi, to serve as an antimicrobial HEA [18]. The study revealed that this alloy demonstrated remarkable antibacterial properties when compared to conventional 304 stainless steel and 304 stainless steel coating with Cu. Furthermore, the study indicated a significant reduction, nearly 99.99 % in antibacterial activity attributed to the release of copper ions from the HEA samples. Ren *et al*. [19] conducted a study on the design and preparation of copper-based HEAs (Cu-HEAs), specifically $Co_{0.4}FeCr_{0.9}Cu_x$, for antibacterial applications. The research delved into the antibacterial mechanism of Cu in HEAs, along with its effects on microstructures, mechanical properties, corrosion resistance, and antibacterial behavior. The results revealed that the Cu-HEAs exhibited a 99.97% antibacterial rate against *E. coli* and a 99.96% antibacterial rate against *S. aureus* after 24 hours. The antibacterial efficacies of CoCrCuFeNi HEA using both ingot metallurgy HEA (IM-HEA) and selective laser melting-HEA (SLM-HEA) surfaces were evaluated and compared to 304 stainless steel surfaces [17]. The results of this study indicated that the HEA surfaces had lower

bacterial colony-forming units compared to the stainless-steel surface. Notably, SLM-HEA exhibited superior antibacterial properties compared to traditional IM-HEA, with a 90% and 98% improvement against *S. aureus* and *E. coli*, respectively. Furthermore, the SLM-HEA surface demonstrated excellent anti-biofilm formation capabilities. However, since SLM involves a laser-melting powder re-curing process, it poses challenges in fully eliminating voids that could potentially arise between the powder particles during the melting phase.

Laser cladding (LC) is a surface modification technique used to produce thin coatings or layers that exhibit excellent surface characteristics or repair surface defects. LC involves the use of a high-power density laser beam as a heat source following a predetermined path on the substrate while feeding coating material powder onto it. This results in the rapid melting of the substrate's surface, with the molten powder and substrate combining and solidifying quickly within the molten pool [20–22]. This method enables the generation of highly durable coatings or layers on the substrate, which is vital for conserving resources and producing high-quality components with desirable surface properties. Therefore, surface treatment is a critical aspect of manufacturing [23].

Minimal energy density was suggested by Gao, Jingbo, *et al*. [15, 22] with a value of 0.066 J.mm−3 applied to coat or treat the stainless steels, as there was typically little to no mixing between the substrate and the clad material. The utilization of LC offers the advantage of efficiently altering the surface properties of the substrate material while minimizing energy consumption. This innovative technique is used for material surface modification and provides several benefits, including the ability to select the most suitable combination of substrate and coating materials and an eco-friendly approach. Hence, LC has commonly been employed as a technique for material coating purposes [24, 25].

The challenge with utilizing stainless steel for medical purposes lies in its surfaces, which have limited ability to inhibit bacterial growth and survival due to the absence of inherent antibacterial properties. Therefore, this study enhances the antibacterial efficacy of stainless-steel surfaces by coating them with CoCrCuFeNi HEA via the LC process.

2.0 METHODOLOGY

2.1 High-entropy Alloy Preparation

In this study, we utilized a powder mixture of pre-alloyed CoCrFeNi and Cu, boasting a purity of 99.8% by weight. The SEM images of pre-alloyed CoCrFeNi and Cu powders are depicted (Figure 1). Table 1 presented the quasi-equiatomic composition of the CoCrFeNi high entropy alloy, demonstrating that the elemental components of the material are approximately equimolar. This balanced composition ensures that each element contributes nearly to the overall composition, resulting in a near-uniform distribution of these elements within the coating.

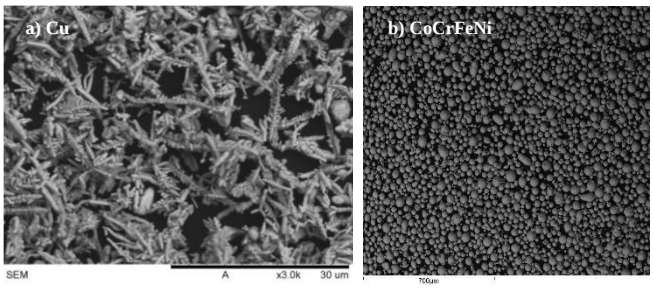

Figure 1 (a) SEM image of Cu and (b) SEM image of pre-alloyed CoCrFeNi

Table 2 Atomic and weight percentage of the elements in CoCrFeNi powder determined using electron microscopy

No.	Element	Weight%	Weight%σ	Atomic
1	Aluminum	2.842	0.727	5.712
2	Chromium	28.973	2.011	30.222
3	Iron	24.259	2.189	23.56
4	Cobalt	21.27	2.506	19.575
5	Nickel	22.657	2.111	20.931

2.2 Powder Paste Preparation

A solution of Polyvinyl alcohol (PVA) was prepared by stirring 13% PVA powder by weight in deionized water for 20 minutes to achieve uniformity. The solution was then heated on a hot plate to a temperature of 90° C for 20 minutes to ensure complete dissolution of the PVA powder. Subsequently, the PVA solution was then gradually combined with 70% by weight of premixed CoCrFeNi and Cu powder, added incrementally. The premixed CoCrFeNi and Cu powder was prepared in a weight ratio of 78:22 (CoCrFeNi:Cu). The mixing was performed manually using a glass rod until a uniform paste was achieved [26]. The resultant paste was then applied to the surface of the stainless-steel substrate, measuring 10mm X 10mm X 3mm for the LC process. A 3D-printed plastic mould was used to maintain a uniform paste thickness of 1 mm. (Figure 2) illustrates the plastic mould, the stainless_steel substrate and the application of the paste to the substrate.

Figure 2 The plastic, stainless steel substrate and paste applied to stainless-steel surface

2.3 Sample Preparation and Characterizations

The LC system, as depicted in (Figure 3), comprises argon gas, a laser cladding head, a water-cooling system, and a fiber laser system. The scanning pattern of the LC was arranged in horizontal parallel lines with a hatch spacing of 1.4 mm and a diameter of 2 mm on the surface of the stainless-steel sample. For the antibacterial work, three samples were compared: an uncoated 304 stainless steel (SS), an SS coated with CoCrFeNi (SS-CoCrFeNi), and an SS coated with CoCrCuFeNi (SS-CoCrCuFeNi). The laser cladding process was carried out on SS-CoCrFeNi and SS-CoCrCuFeNi samples at a laser power of 300 W and a scanning speed of 1600 mm/min, as shown (Figure 4).

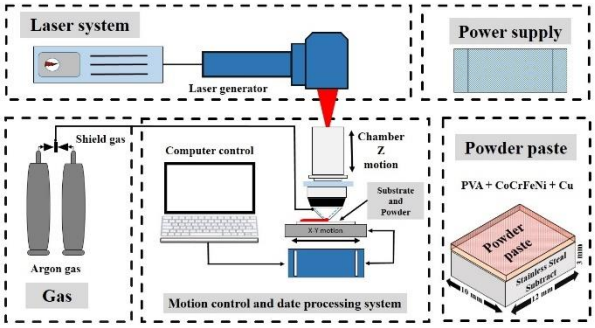

Figure 3 The LC system

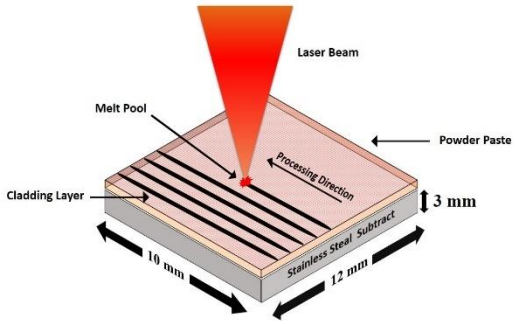

Figure 4 Laser cladding process

This procedure was performed to promote the growth of the bacterial colonies. The colonies were then incubated for 24 hours at 37°C.

The samples underwent analysis using Scanning Electron Microscopy (SEM), X-ray Diffraction Analysis (XRD), Energy Dispersive X-ray Analysis (EDX), and Vickers Hardness test. These techniques were employed to investigate and comprehend the variations in antibacterial efficacy among the prepared samples.

2.4 Bacterial Growth Conditions and Preparation

The antibacterial assays were performed following the procedures previously reported by Gao *et al*. [19]. *Escherichia coli (E. coli)*, a gram-negative bacterium, and *Staphylococcus aureus (S. aureus)*, a gram-positive bacterium, were cultured at the College of Science, Mustansiriyah University, located in Baghdad, Iraq [27, 28].

Bacterial growth was initiated by supplementing 10 ml of sterilized tryptone soya broth (TSB) with the bacteria. The mixture was then incubated at 37° C for 24 hours. The cultured bacteria were subsequently diluted to achieve a bacterial suspension concentration of approximately 10^4 (CFU)/ml. The sterilization process involved an autoclave at a temperature of 121° C and a pressure of 15 lbs for 15 minutes. The process was followed by a cooling phase to a temperature range of (45 to 50)° C [29]. In the inoculation process, a volume of 20µm from the diluted bacterial suspension was applied to the SS, SS-CoCrFeNi and SS-CoCrCuFeNi samples. All the samples were transferred to separate Petri dishes, and the bacterial coverage was evenly distributed on the surfaces with the cover slips as shown in (Figure 5(a)). The samples were then incubated for 24 hours at a temperature of 37° C. Subsequently, the samples were transferred into 10ml tubes, each containing 10ml of sterile phosphate-buffered saline (PBS). (Figure 5(b)) shows the SS, SS-CoCrFeNi, and SS-CoCrCuFeNi samples submerged in the PBS. These tubes underwent vortexing for 20 seconds to facilitate release of bacteria into the PBS solution. This step was repeated three times for each sample [28]. Upon completion, the bacteria were extracted from the Falcon tubes using cotton swabs and transferred to Petri dishes containing the cultured media.

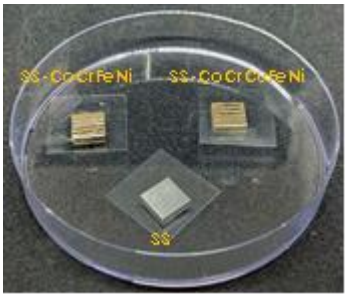

(a)

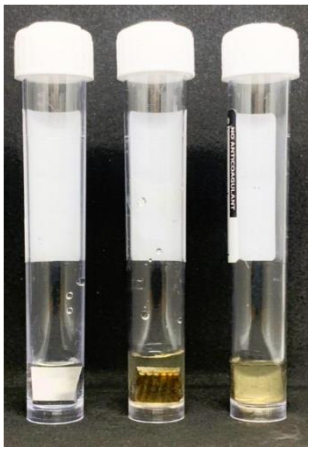

(b)

Figure 5 (a) Samples with cover slip. (b) Samples into tube: SS, SS-CoCrFeNi, and SS-CoCrCuFeNi respectively

The images of colonies were captured using a digital camera. The *ImageJ* software was employed to count the colony_forming units (CFU). The antibacterial efficacy (%) of each sample was determined using Equation (1.1).

$$\text{Antibacterial rate (\%)} = \frac{N_{control} - N_{sample}}{N_{control}} X100 \quad (1.1)$$

Where N_{sample} represents the CFU count of the average bacterial colonies on different SS-CoCrCuFeNi and SS-CoCrFeNi, $N_{control}$ is the CFU count of the SS sample.

3.0 RESULTS AND DISCUSSION

3.1 Elemental, microstructures, and mechanical properties of the samples

XRD generates a series of diffraction peaks with varying positions and intensities, which correspond to the crystal structure through phase analysis [30, 31]. The SS, SS-CoCrFeNi, and SS-CoCrCuFeNi samples were examined using XRD. (Figure 6) depicts the XRD results of the samples, with the following symbols representing different elements in the spectrum: Iron (Fe) is denoted by (*), Cobalt (Co) by (∇), Chromium (Cr) by (◯), Nickel (Ni) by (•) and Copper (Cu) by (⊗) [32– 35]. The XRD analysis revealed increments in the peak intensities for each sample as follows: SS sample at (111), (110), (200), and (311); SS-CoCrFeNi sample at (111), (200), and (311); and SS-CoCrCuFeNi sample at (111), (200), and (311), respectively [36–38].

Based on the XRD pattern, the highest intensity at position (200) for both the SS-CoCrFeNi and SS-CoCrCuFeNi could be attributed two factors. Firstly, the crystal structures of the SS-CoCrCuFeNi materials were enhanced, leading to a more organized, homogeneous, and less flawed crystal lattice. This improvement facilitated the achievement of stable states between the fracture and cold welding of the powder particles. As a result, there was more effective scattering of X-ray, yielding in a stronger diffraction signal**.** Secondly, this could be attributed to the large grain size of the material. It can be inferred that the XRD pattern generated was a result of the mechanical process of complete alloying of the SS-CoCrFeNi and SS-CoCrCuFeNi via diffusion [39]. As depicted in (Figure 7-9) the larger the grain size of the coating material, the higher the intensity peak in the XRD pattern due to the enhancement of the diffraction signal.

The energy dispersive X-ray spectroscopy (EDX) analysis of the elemental composition of SS, SS-CoCrFeNi, and SS-CoCrCuFeNi samples is presented in the mapping results. (Figure 7(c)) reveals that the specimens exhibited a diverse range of elemental composition. Upon examining the composition distribution maps of the specimens, it was observed that the surface region of the SS exhibited a significant enrichment in Ni, Cr, and Fe. (Figure 8(c)) presents the elemental composition of SS-CoCrFeNi. The composition distribution maps of the specimen indicate a significant enrichment of Cr, Co, Fe, and Ni in the surface region of SS-CoCrFeNi. However, (Figure 9(c)) shows that the surface of SS-CoCrCuFeNi was notably enriched in Cu, and Ni elements in the same region, though not as significant as the enrichment of Cr and Fe.

Table 2 presents the elemental percentages of each sample. The elemental percentages for Cr, Fe, and Ni in the SS sample were 20.6%, 69.7%, and 7.4%, respectively. For the SS-CoCrFeNi sample, the percentages for Co, Cr, Fe and Ni were 22.8%, 26.6%, 26.1%, and 23.7%, respectively. In the SS-CoCrCuFeNi sample, the elemental percentages for Cu, Co, Cr, Fe, and Ni were 15.6%, 20.4%, 18.9%, 24.3% and 18.1%, respectively. These percentages reflect a nearly equimolar elemental content, further confirming the formation of the high entropy alloy coating.

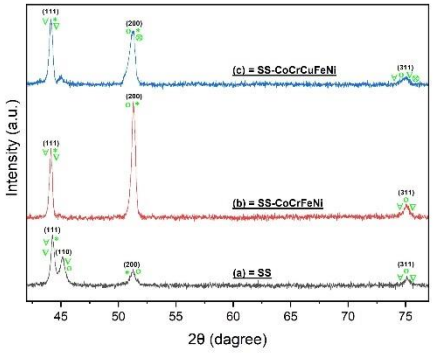

Figure 6 The XRD of the (a) SS, (b) SS-CoCrFeNi and (c) SS-CoCrCuFeNi samples

Table 2 Elemental percentage of the (a) SS, (b) SS-CoCrFeNi, and (c) SS-CoCrCuFeNi samples

No.	Alloy	Cu	Co	Cr	Fe	Ni
1	SS			20.6	69.7	7.4
2	SS-CoCrFeNi		22.8	26.6	26.1	23.7
3	SS-CoCrCuFeNi	15.6	20.4	18.9	24.3	18.1

Figure 7-9 displays the SEM images, with (Figure 7 (a-b)) showing the surface morphology of the stainless steel sample, portraying typical characteristics such as the presence of cracks, pits, and holes. As a result, the presence of such pits and holes on the stainless steel surface may lead to corrosion. When stainless steel is subjected to both tensile stress and a corrosive environment, it becomes prone to stress corrosion cracking, which arises from the interplay between mechanical stress and chemical reactions, resulting in crack formation. In (Figure 8 (a-b)), the SS-CoCrFeNi coating surface morphology was lacked connectivity with the substrate. The coating was presented with cracks and pits. However, as shown in (Figure 9 (a-b)),

the SS-CoCrCuFeNi sample exhibited a more uniform distribution of elements, which is a common observation in the SEM images. This sample displayed fewer pits and cracks on its surface, leading to its high hardness, antibacterial properties, and lower susceptibility to corrosion.

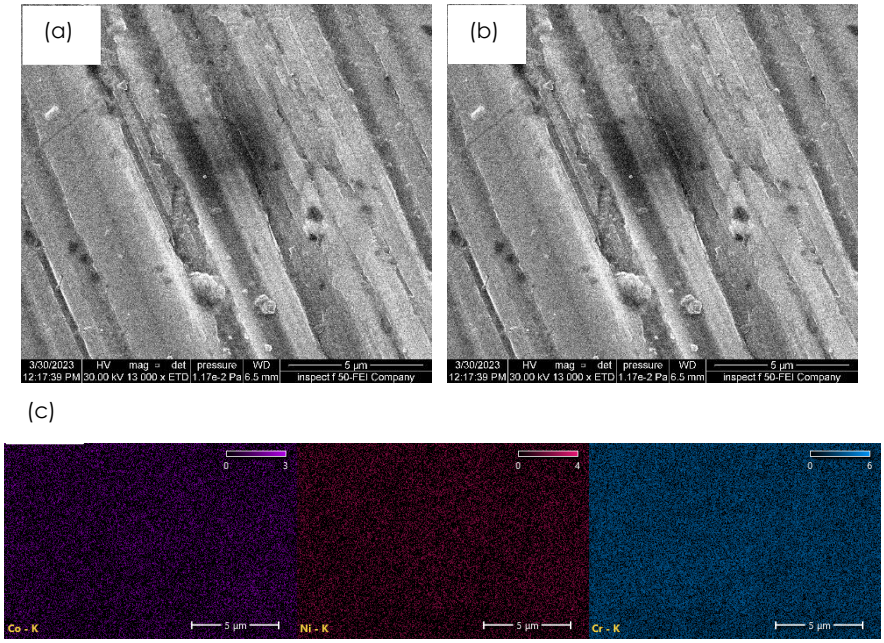

Figure 7 (a) and (b) SEM SS, and (c) EDX SS samples

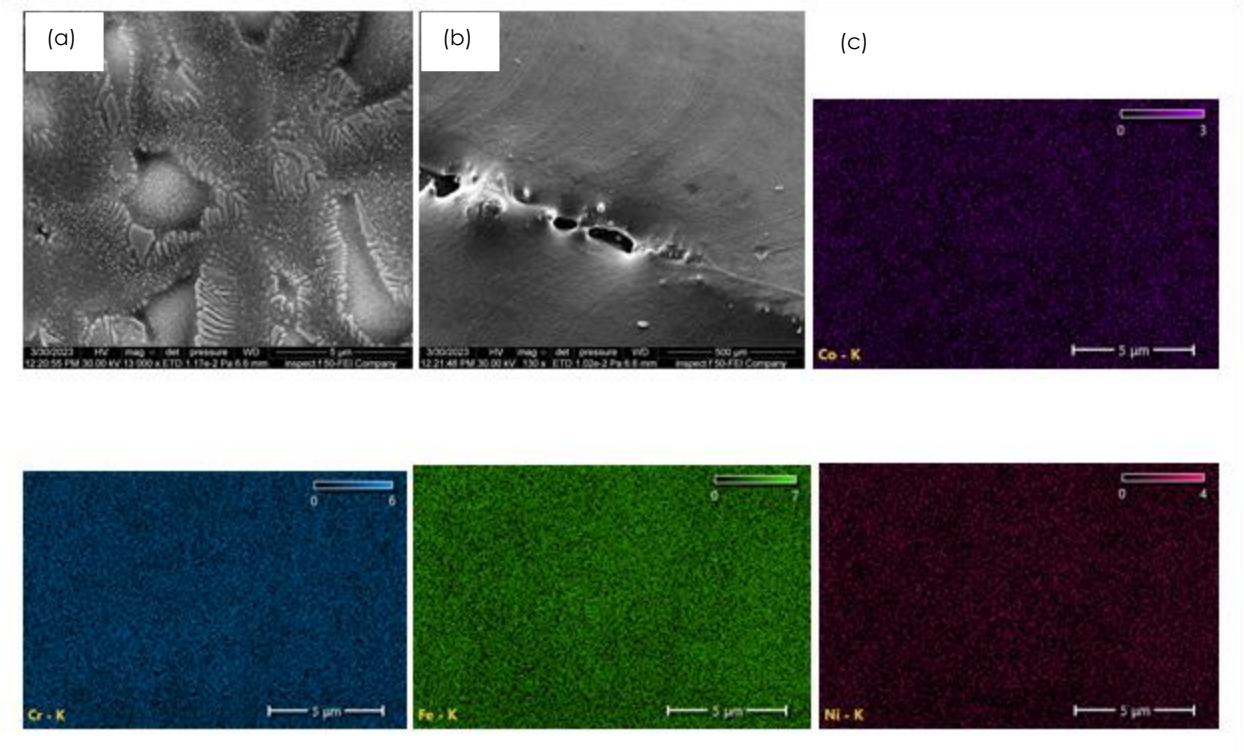

Figure 8 (a) and (b) SEM SS-CoCrFeNi, and (c) EDX SS-CoCrFeNi samples

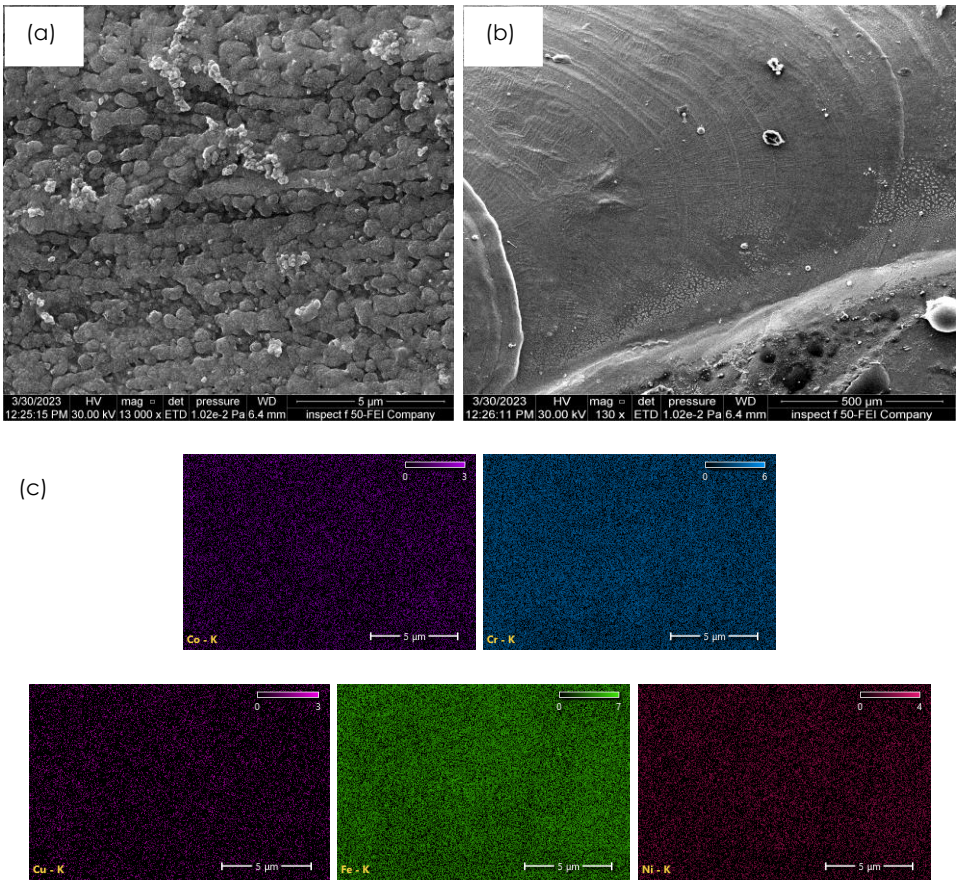

Figure 9 (a) and (b) SEM SS-CoCrCuFeNi, and (c) EDX SS-CoCrCuFeNi samples

(Figure 10) displays the hardnesses of SS, SS-CoCrFeNi, and SS-CoCrCuFeNi samples, as measured by the Vicker's hardness test. In terms of the hardness of the measured samples, the SS sample exhibits an average hardness of 256.6 HV with a relatively low standard deviation of 16.9 HV. This result indicates consistent hardness values across various points on the stainless-steel surface. The SS-CoCrFeNi sample shows a significantly increases in hardness, with an average hardness of 300.6 HV. However, the relatively high standard deviation of 75.3 HV suggests a considerable variability in hardness values within the CoCrFeNi alloy coating. The SS-CoCrCuFeNi sample exhibits the highest average hardness at 352.0 HV, with a low standard deviation of 28.9 HV as depicted in (Figure 10). The low standard deviation of SS-CoCrCuFeNi sample indicates a more consistent coating hardness compared to SS-CoCrFeNi. Furthermore, it demonstrates a higher average hardness of 352.0 HV compared to the average hardness of SS-CoCrFeNi at 300.6 HV. This can be attributed to the more uniform distribution of elements observed. The SS-CoCrCuFeNi sample shows fewer pits and cracks on its surface, which results in superior hardness. This is evident in the SEM images, as shown in (Figure 9 (b)).

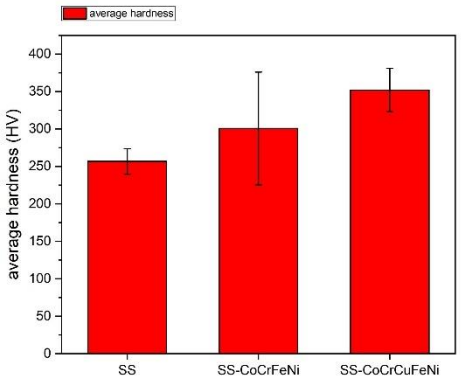

Figure 10 The hardness of SS, SS-CoCrFeNi and SS-CoCrCuFeNi samples

3.2 Antibacterial Efficacy

The antibacterial efficacy of the samples was evaluated by incubating them with *S. aureus* and *E. coli* for a period of 24 hours. (Figure 11 (a-c)) illustrates the antibacterial performance of three distinct samples (a) SS, (b) SS-CoCrFeNi, and (c) SS-CoCrCuFeNi. The findings suggest that the highest number of bacterial colonies of *S. aureus* and *E. coli* were observed on the surfaces of SS. This was followed by SS-CoCrFeNi, which exhibited fewer colonies than SS. In contrast, no bacterial colonies of *S. aureus* and *E. coli* were detected on the surfaces of SS-CoCrCuFeNi. Consequently, these results suggest enhanced antibacterial properties with the transition from SS to SS-CoCrFeNi and SS-CoCrCuFeNi coatings. The SS-CoCrFeNi HEA demonstrated an antibacterial rate of approximately 40% against *E. coli* and 93% against *S. aureus,* as illustrated in (Figure 11 (b)). Previous research has highlighted variations in the antibacterial properties of elements such as cobalt (Co), chromium (Cr), and iron (Fe), particularly in terms of their effectiveness against various bacteria. These elements also contribute to enhancing corrosion resistance, hardness, and formation [40,41]. However, the SS-CoCrCuFeNi HEA demonstrated an antibacterial rate of approximately 89% against *E. coli* and 98% against *S. aureus*, as depicted in (Figure 11 (c)). Consequently, the assessment of SS-CoCrCuFeNi_HEA coating revealed its superior antibacterial efficacy, which can be ascribed to the presence of Cu ions in the alloy. Cu ions were observed to exert a potent bactericidal effect against both *S. aureus* and *E. coli*. Selective laser melting has exhibited exceptional antibacterial performance. Moreover, compared to the IM-HEA, the SLM-HEA demonstrated approximately 90% antibacterial activity against *S. aureus* and over 75% antibacterial activity against *E. coli*, as reported by Gao, J., Jin, Y., Fan [17].

4.0 CONCLUSION

Uniform CoCrFeNi, and CoCrCuFeNi HEA coatings on stainless steel surfaces were fabricated through laser cladding and in-situ alloying. An investigation was conducted on the microstructure, hardness properties, and antibacterial activity of the SS, SS-CoCrFeNi, and SS-CoCrCuFeNi and the results were subsequently compared. Based on the findings, the following conclusions were drawn:

The hardness properties of the SS-CoCrCuFeNi material exhibited a significant improvement compared to both the SS and SS-CoCrFeNi. This marked enhancement in hardness properties underscores the superior performance of SS-CoCrCuFeNi material relative to the other alloys.

The antibacterial properties of the SS-CoCrCuFeNi material were observed to be significantly superior to those of the uncoated stainless steel against *E. coli* and *S. aureus*. This can be attributed to the concentration of copper ion released from the SS-CoCrCuFeNi material. This outcome underscores the potential of laser cladding in fabricating durable coating with improved antibacterial capabilities for medical applications.

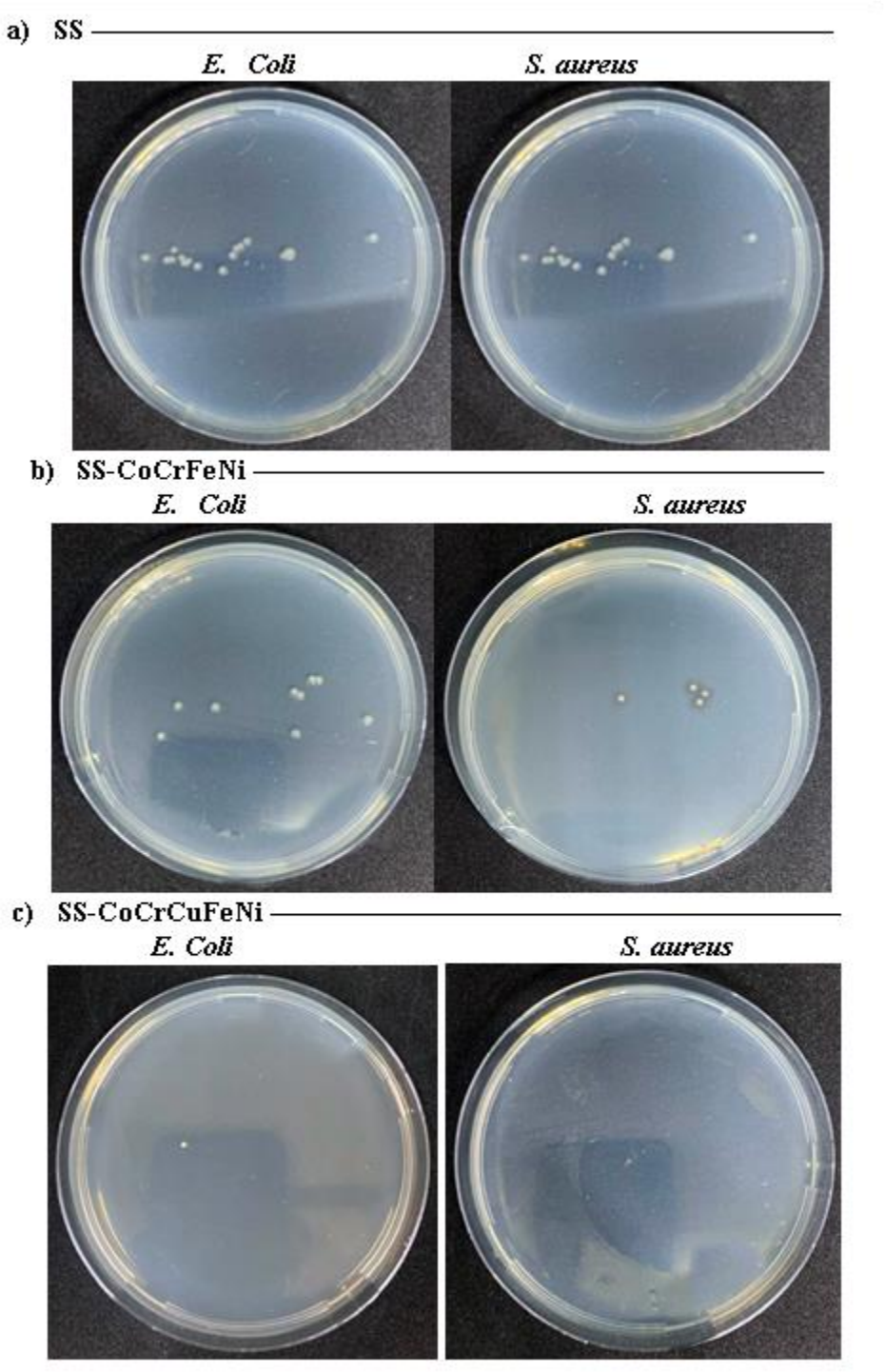

Figure 11 The bacteria test, (a) SS, (b) SS-CoCrFeNi, and (c) SS-CoCrCuFeNi samples

Acknowledgement

This research was supported by the Ministry of Education Malaysia and Universiti Teknologi Malaysia through UTM RA Iconic Grant, cost center no. Q.J130000.4354.09G60 and UTM Encouragement Research, cost center no. Q.J130000.3854.31J74. The main author also wishes to thank Dr. Mohammed F. Almarjani, Mustansiriyah University, Baghdad, Iraq for his support in finishing this work.

Conflicts of Interest

The author(s) declare(s) that there is no conflict of interest regarding the publication of this paper.

References

[1] Adlhart, C., Verran, J., Azevedo, N. F., Olmez, H., Keinänen-Toivola, M. M., Gouveia, I., Melo, L. F. and Crijns, F. 2018. Surface Modifications for Antimicrobial Effects in the Healthcare Setting: A Critical Overview. *Journal of Hospital Infection*. 99(3): 239-249.

[2] Lewis, D. 2021. COVID-19 Rarely Spreads through Surfaces. So Why are We Still Deep Cleaning. *Nature*. 590(7844): 26-28.

[3] Owusu, E., Asane, F. W., Bediako-Bowan, A. A. and Afutu, E. 2022. Bacterial Contamination of Surgical Instruments used at the Surgery Department of a Major Teaching Hospital in a Resource-limited Country: An Observational Study. *Diseases*. 10(4): 81.

[4] Cloutman-Green, E., Canales, M., Zhou, Q., Ciric, L., Hartley, J.C. and McDonnell, G. 2015. Biochemical and Microbial Contamination of Surgical Devices: A Quantitative Analysis. American Journal of Infection Control. 43(6): 659-661.

[5] Panta, G., Richardson, A. K. and Shaw, I. C. 2019. Effectiveness of Autoclaving in Sterilizing Reusable Medical Devices in Healthcare Facilities. *The Journal of Infection in Developing Countries*. 13(10): 858-864.

[6] de Melo Costa, D., de Oliveira Lopes, L. K., Hu, H., Tipple, A. F. V. and Vickery, K. 2017. Alcohol Fixation of Bacteria to Surgical Instruments Increases Cleaning Difficulty and may Contribute to Sterilization Inefficacy. *American Journal of Infection Control*. 45(8): e81-e86.

[7] Nan, L., Xu, D., Gu, T., Song, X. and Yang, K. 2015. Microbiological Influenced Corrosion Resistance Characteristics of a 304L-Cu Stainless Steel against Escherichia coli. *Materials Science and Engineering: C*. 48: 228-234.

[8] Zhao, J., Zhai, Z., Sun, D., Yang, C., Zhang, X., Huang, N., Jiang, X. and Yang, K. 2019. Antibacterial Durability and Biocompatibility of Antibacterial-passivated 316L Stainless Steel in Simulated Physiological Environment. *Materials Science and Engineering: C*. 100: 396-410.

[9] Axinte, D., Guo, Y., Liao, Z., Shih, A. J., M'Saoubi, R. and Sugita, N. 2019. Machining of Biocompatible Materials—Recent Advances. *CIRP Annals*. 68(2): 629-652.

[10] Cantor, B., Chang, I. T. H., Knight, P. and Vincent, A. J. B. 2004. Microstructural Development in Equiatomic Multicomponent Alloys. *Materials Science and Engineering: A*. 375: 213-218.

[11] Yeh, J. W., Chen, S. K., Lin, S. J., Gan, J. Y., Chin, T. S., Shun, T. T., Tsau, C. H. and Chang, S. Y. 2004. Nanostructured High-entropy Alloys with Multiple Principal Elements: Novel Alloy Design Concepts and Outcomes. *Advanced Engineering Materials*. 6(5): 299-303.

[12] Yeh, J. W. 2013. Alloy Design Strategies and Future Trends in High-entropy Alloys. *Jom*. 65: 1759-1771.

[13] Wu, H., Zhang, S., Wang, Z. Y., Zhang, C. H., Chen, H. T., & Chen, J. 2022. New Studies on Wear and Corrosion Behavior of Laser Cladding FeNiCoCrMox High Entropy Alloy Coating: The Role of Mo. *International Journal of Refractory Metals and Hard Materials*. 102: 105721.

[14] Cheng, J., Liu, D., Liang, X., & Chen, Y. 2015. Evolution of Microstructure and Mechanical Properties of In Situ Synthesized TiC–TiB2/CoCrCuFeNi High Entropy Alloy Coatings. *Surface and Coatings Technology*. 281: 109-116.

[15] Jiang, P. F., Zhang, C. H., Zhang, S., Zhang, J. B., Chen, J., & Liu, Y. 2020. Fabrication and Wear Behavior of TiC Reinforced FeCoCrAlCu-based High Entropy Alloy Coatings by Laser Surface Alloying. *Materials Chemistry and Physics*. 255: 123571.

[16] Xiao, D. H., Zhou, P. F., Wu, W. Q., Diao, H. Y., Gao, M. C., Song, M., & Liaw, P. K. 2017. Microstructure, Mechanical and Corrosion Behaviors of AlCoCuFeNi-(Cr, Ti) High Entropy Alloys. *Materials & Design*. 116: 438-447.

[17] Gao, J., Jin, Y., Fan, Y., Xu, D., Meng, L., Wang, C., ... & Wang, F. 2022. Fabricating Antibacterial CoCrCuFeNi High-Entropy Alloy via Selective Laser Melting and In-situ Alloying. *Journal of Materials Science & Technology*. 102: 159-165.

[18] Zhou, E., Qiao, D., Yang, Y., Xu, D., Lu, Y., Wang, J., ... & Wang, F. 2020. A Novel Cu-bearing High-entropy Alloy with Significant Antibacterial Behavior Against Corrosive Marine Biofilms. *Journal of Materials Science & Technology*. 46: 201-210.

[19] Ren, G., Huang, L., Hu, K., Li, T., Lu, Y., Qiao, D., ... & Liaw, P. K. 2022. Enhanced Antibacterial Behavior of a Novel Cu-bearing High-entropy Alloy. *Journal of Materials Science & Technology*. 117: 158-166.

[20] Sharma, A., McQuillan, A. J., A Sharma, L., Waddell, J. N., Shibata, Y., & Duncan, W. J. 2015. Spark Anodization of Titanium–zirconium Alloy: Surface Characterization and Bioactivity Assessment. *Journal of Materials Science: Materials in Medicine*. 26: 1-11.

[21] Zhang, H., Pan, Y., & He, Y. Z. 2011. Synthesis and Characterization of FeCoNiCrCu High-entropy Alloy Coating by Laser Cladding. *Materials & Design*. 32(4): 1910-1915.

[22] Wang, L., Gao, Z., Wu, M., Weng, F., Liu, T., & Zhan, X. 2020. Influence of Specific Energy on Microstructure and Properties of Laser Cladded FeCoCrNi High Entropy Alloy. *Metals*. 10(11): 1464.

[23] Siddiqui, A. A., & Dubey, A. K. 2021. Recent Trends In Laser Cladding and Surface Alloying. *Optics & Laser Technology*. 134: 106619.

[24] Burakowski, T., & Wierzchon, T. 1998. *Surface Engineering of Metals: Principles, Equipment, Technologies*. CRC Press.

[25] Tamanna, N., Crouch, R., & Naher, S. 2019. Progress in Numerical Simulation of the Laser Cladding Process. *Optics and Lasers in Engineering*. 122: 151-163.

[26] Renteria, A., Diaz, J. A., He, B., Renteria-Marquez, I. A., Chavez, L. A., Regis, J. E., ... & Lin, Y. 2019. Particle Size Influence on Material Properties of BaTiO3 Ceramics Fabricated using Freeze-form Extrusion 3D Printing. *Materials Research Express*. 6(11): 115211.

[27] Said, L. A. (2020). Biosynthesis and Characterization of Silver Nanoparticles from Pantoea agglomerans and some of Their Antibacterial Activities. *Al-Mustansiriyah Journal of Science*. 31(3): 1-5.

[28] Jabber, S. H., Hussain, D. H., Rheima, A. M., & Faraj, M. 2019. Comparing Study of CuO Synthesized by Bl Activity. *Al-Mustansiriyah Journal of Science*. 30(1): 94-8.

[29] Al-Hashimi, A. M. 2018. Biodegradation Effect of some Bacterial Isolates on some Endocrine Disruptors (EDCS). Endocrine. 17: 01.

[30] Kozlovskiy, A. L., Kenzhina, I. E., & Zdorovets, M. V. 2020. FeCo–Fe_2CoO_4/Co_3O_4 Nanocomposites: Phase Transformations as a Result of Thermal Annealing and Practical Application in Catalysis. *Ceramics International*. 46(8): 10262-10269.

[31] Zdorovets, M. V., & Kozlovskiy, A. L. 2020. Study of Phase Transformations in Co/$CoCo_2O_4$ Nanowires. *Journal of Alloys and Compounds*. 815: 152450.

[32] Jian, Y., Huang, Z., Liu, X., Sun, J., & Xing, J. 2020. Microstructure, Mechanical Properties and Toughening Mechanism of Directional Fe2B Crystal in Fe-B Alloy with Trace Cr Addition. *Journal of Materials Science & Technology*. 57: 172-179.

[33] Ehsan, M. A., Hakeem, A. S., & Rehman, A. 2020. Hierarchical Growth of CoO Nanoflower Thin Films Influencing the Electrocatalytic Oxygen Evolution Reaction. *Electrocatalysis*. 11: 282-291.

[34] Shen, L., & Wang, N. 2011. Effect of Nitrogen Pressure on the Structure of Cr-N, Ta-N, Mo-N, and WN Nanocrystals Synthesized by Arc Discharge. *Journal of Nanomaterials*. 2011: 1-5.

[35] Pandey, V. K., Shivam, V., Sarma, B. N., & Mukhopadhyay, N. K. 2020. Phase Evolution and Thermal Stability of Mechanically Alloyed CoCrCuFeNi High Entropy Alloy. *Materials Research Express*. 6(12): 1265b9.

[36] Chen, M., Xing, S., Liu, H., Jiang, C., Zhan, K., & Ji, V. 2020. Determination of Surface Mechanical Property and Residual Stress Stability for Shot-peened SAF2507 Duplex Stainless Steel by In Situ X-ray Diffraction Stress Analysis. *Journal of Materials Research and Technology*. 9(4): 7644-7654.
[37] Lei, N., Li, X., Li, W., Zhang, G., Wei, R., Wang, T., ... & Chen, C. 2022. A Fe-rich Co-free High Entropy Alloy with Excellent Mechanical and Anti-bacterial Properties in Cold-rolled State. *Materials Letters*. 328: 133139.
[38] Zhang, L. J., Fan, J. T., Liu, D. J., Zhang, M. D., Yu, P. F., Jing, Q., ... & Liu, R. P. 2018. The Microstructural Evolution and Hardness of the Equiatomic CoCrCuFeNi High-entropy Alloy in the Semi-solid State. *Journal of Alloys and Compounds*. 745: 75-83.
[39] Jamil, N. A. B. M., Mohamaddiah, A. H. B., Azami, M. H. B., & Nordin, N. H. 2023. High Entropy Alloy as Metal Additive for Hybrid Rocket Propellant. *Materials Today: Proceedings*. 75: 140-146.
[40] Aisida, S. O., Ugwu, K., Agbogu, A., Ahmad, I., Maaza, M., & Ezema, F. I. 2023. Synthesis of Intrinsic, Manganese and Magnesium Doped Cobalt Ferrite Nanoparticles: Physical Properties for Antibacterial Activities. *Hybrid Advances*. 100049.
[41] Adnan, W. G., & Mohammed, A. M. 2023. Green Synthesis of Chromium Oxide Nanoparticles for Anticancer, Antioxidant and Antibacterial Activities. *Inorganic Chemistry Communications*. 111683.